JOURNAL OF GEOPHYSICAL RESEARCH, VOL. 100, NO. D8, PAGES 16,395–16,414, AUGUST 20, 1995

Precipitation and radiation modeling in a general circulation model: Introduction of cloud microphysical processes

Olivier Boucher and Hervé Le Treut

Laboratoire de Météorologie Dynamique du CNRS, Ecole Normale Supérieure, Paris, France

Marcia B. Baker

Geophysics Program, University of Washington, Seattle

Abstract. Cloud microphysical processes are introduced in the precipitation parameterization of a general circulation model (GCM). Three microphysical processes are included in this representation of warm cloud precipitation: autoconversion of droplets, collection of droplets by falling raindrops, and evaporation of raindrops falling in clear sky. The mean droplet radius, r, is calculated from the cloud water mixing ratio, which is computed in the model, and the cloud droplet number concentration, N, which is prescribed. The autoconversion rate is set to zero for $r < r_0$, a prescribed threshold mean droplet radius. We investigate the model sensitivity to r_0 and to N, the cloud droplet concentration, which is linked to the concentration of cloud condensation nuclei and is likely to vary. We find that an increase in N leads to an increase in the amount of cloud water stored in the atmosphere. In further experiments the mean droplet radius used in the parameterization of cloud optical properties is calculated in the same way as in the precipitation parameterization in order to bring more consistency between the different schemes. We again investigate the model sensitivity to r_0 and to N and we find that an increase in N significantly enhances cloud albedo.

1. Introduction

It is now well established that clouds play a significant role in the climate system, especially through their interactions with solar and terrestrial radiation [*Arking*, 1991; *Slingo*, 1990]. However, the processes which control cloud occurrence and cloud optical properties are still poorly understood and imperfectly represented in climate models. It is important to improve their parameterization since large uncertainties (larger than the expected man-made greenhouse effect) remain concerning their radiative effects [*Cess et al.*, 1990]. Indeed, clouds may be at the origin of many feedback effects which are able to increase or dampen significantly a global warming. In spite of this, most sensitivity studies to date have been limited to macroscale feedbacks since the parameters affected by microscale processes, such as the cloud droplet radius, are generally prescribed at a fixed value within general circulation models (GCM) or are ignored. *Liou and Ou* [1989] proposed for instance that, because precipitation is increased in doubling CO_2 GCM experiments, there could be a reduction in the cloud condensation nuclei (CCN) concentration through wet removal of atmospheric aerosols and consequently an increase in cloud droplet size.

Apart from their importance as a potential agent of climate feedback, microscale cloud parameters also need to be included in future parameterizations because, over land at least, pollution is shown to increase the number of CCN, a parameter crucial to the cloud albedo. An increase in cloud droplet number concentration at a given liquid water content yields more and smaller droplets, which, in turn, increases the cloud albedo [*Twomey*, 1974, 1977; *Twomey et al.*, 1984; *Charlson et al.*, 1987]. Also, *Albrecht* [1989] showed that the CCN concentration was an important parameter for the maintenance of marine boundary layer clouds through drizzle formation.

Hunt [1982] studied the climatic impact of increasing low-level cloud albedo in a hemispheric general circulation model and obtained a reduction in surface temperature while dynamical changes were also observed. This ad hoc increase in cloud albedo is to be seen as an idealized way of modeling changes in the cloud droplet size distribution. *Ghan et al.* [1990], in an attempt to test the CCN-cloud albedo-climate hypothesis of *Charlson et al.* [1987], showed that a fourfold increase in marine cloud droplet concentration translated into a 1.7% increase in global albedo. Recently, *Kiehl* [1994] studied the effect on the simulated climate of reducing the effective droplet size over land in the National Center for

Paper number 95JD01382.
0148-0227/95/95JD-01382$05.00

Atmospheric Research (NCAR) climate model. He observed a reduction in surface-absorbed solar radiation and temperature over continents. Changes in the precipitation distribution and in the geopotential height field were also identified. The aim of the present study is slightly different: it consists in introducing a simple parameterization of some cloud microphysical processes (precipitation and radiation) into a GCM, and examining the sensitivity of cloud-related quantities to changes in the cloud microphysical parameters.

The outline of this study is as follows: section 2 is a brief presentation of the GCM used in this study. In section 3 we analyze the theoretical framework of the precipitation parameterization. Results and their sensitivity to the cloud droplet concentration are discussed in section 4. An attempt to bring consistency between the parameterizations of the precipitation and radiative transfer, through a single definition of the cloud droplet radius, is described in section 5.

2. LMD GCM Description

The LMD (Laboratoire de Météorologie Dynamique) GCM was first described by *Sadourny and Laval* [1984]. It is a grid point model with 64 points evenly spaced in longitude, 50 points evenly spaced in sine of the latitude, and 11 σ levels. The time step for the dynamics is 6 min and the physical processes are computed every five time steps (30 min). Cycle 6 of the model is used for the present study. A rather advanced ground physics parameterization [*Ducoudré et al.*, 1993] is now included, with a representation of the hydrological role of the vegetation. The radiative parameterization is an improved version of the codes described in *Fouquart and Bonnel* [1980] (solar radiation) and *Morcrette* [1991] (terrestrial radiation). The model takes into account the diurnal cycle.

The description of cloudiness in the model is based on a cloud water budget equation in which both the convective and nonconvective water sources are taken into account. The cloud water mixing ratio, q_l, is therefore a model prognostic variable, but a single parameter is used to represent both liquid water and ice.

We use both convective and nonconvective condensation as a source of cloud water. The nonconvective condensation is handled through a simple statistical approach, which allows a single definition of the cloud fraction for the precipitation and radiation schemes. A Kuo scheme and moist adiabatic adjustment are used jointly to predict convective condensation. These adjustment schemes are not well adapted to the prediction of convective water sources: We do not distinguish the transport of water vapour by the convective mass flux from the loss of water vapour by condensation, so that we must define the model level at which the water vapour condensation occurs. We diagnose it as the level where the moisture depletion is largest, which may lower the level of the convective sources of cloud water.

It is useful to note here a numerical peculiarity of the present version of the LMD GCM. We call the convective condensation scheme and the stratiform condensation scheme sequentially, and retain the convective cloud water in the atmosphere before entering the large-scale precipitation scheme. We have therefore complete detrainment of the convective cloud water in the stratiform clouds; or reevaporation of convective cloud water in an unsaturated environment. All types of condensate are handled through the same precipitation routine, which is described in the next section. This is a crude representation of reality because convective cloud water might precipitate before being detrained into a stratiform cloud. More sophisticated convective schemes are required to handle these processes adequately. However this approach remains acceptable here since the aim of this paper is only to test the sensitivity of the model to the precipitation processes within warm clouds. Recent experiments where all convective condensed water is precipitated shows that the overestimation of the total cloud water remains marginal (within 10% of its value) and does not alter the cloud radiative forcing significantly.

It is necessary to describe the stratiform condensation scheme [*Le Treut and Li*, 1991] in more detail, because due to the detrainment of convective cloud water in stratiform clouds, all clouds eventually become stratiform in this version of the model. The scheme uses a simple statistical approach and rests on the idea that the subgrid-scale dynamics may be simply described by large-scale parameters. The model formulation implies that there is no memory of these structures from one time step to the next one. The subgrid probability distribution of total water (water vapor and cloud water) is assumed to be uniform between $q_t - \Delta q$ and $q_t + \Delta q$, where $q_t = q + q_l$ is the grid box average value of the total water mixing ratio and $\Delta q = \gamma\, q_t$ (see Figure 1). Here γ is set to 0.20 in order to get the observed value of global cloudiness. The choice of q_t as the main variable for this description of subgrid scales is natural because it is a conservative variable. At the same time, it indicates that both condensation and reevaporation of cloud water will be taken into account through this scheme. The cloud fraction, f, is defined as the part of the grid box where the total water exceeds the water vapor mixing ratio at saturation.

$$f = \begin{cases} \frac{q_t + \Delta q - q_{\text{sat}}}{2\Delta q} & \text{if } q_{\text{sat}} \in [q_t - \Delta q, q_t + \Delta q] \\ 0 & \text{if } q_{\text{sat}} > q_t + \Delta q \\ 1 & \text{if } q_{\text{sat}} < q_t - \Delta q \end{cases}$$

$$q_{t\text{cloud}} = \begin{cases} \frac{q_{\text{sat}} + q_t + \Delta q}{2} & \text{if } q_{\text{sat}} \in [q_t - \Delta q, q_t + \Delta q] \\ q_t & \text{if } q_{\text{sat}} < q_t - \Delta q \end{cases}$$

$$q_{t\text{clear}} = \begin{cases} \frac{q_{\text{sat}} + q_t - \Delta q}{2} & \text{if } q_{\text{sat}} \in [q_t - \Delta q, q_t + \Delta q] \\ q_t & \text{if } q_{\text{sat}} > q_t + \Delta q \end{cases}$$

If f is positive, then condensation can occur in the cloudy part only, leading to a new in-cloud temperature and cloud water content. Once f is determined, the temperature is averaged over the whole grid box. We note that an increase in total water is partitioned

in three parts increasing the cloud water content, the cloud fraction, and the clear sky humidity, respectively.

Unfortunately, stratus clouds over the oceans are not properly simulated: this is probably not due to the cloud scheme itself, which managed to produce reasonable low cloud distributions when inserted in the European Centre for Medium-Range Weather Forecasts (ECMWF) GCM [*Le Treut and Illari, 1993*], but to the general characteristics of the boundary layer in the LMD GCM, which tends to be too dry near its top.

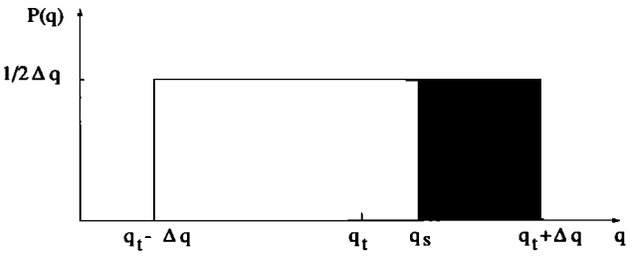

Figure 1. Subgrid distribution density of total water. The darkened area represents the cloudy region.

3. Description of the Precipitation Parameterization

Supercooled water clouds are very common in the atmosphere at temperatures below 0°C but their frequency decreases rapidly with decreasing temperatures, and ice particles are almost always present at −18°C [*Pruppacher and Klett*, 1978]. We assume here that liquid water clouds and ice clouds coexist at temperatures between 0°C and −15°C. At each grid point, liquid water clouds constitute a fraction x, and ice clouds constitute a fraction $1-x$, of the total cloud cover. Here x is equal to 0 for temperatures below −15°C, 1 for temperatures above 0°C, and we assume it varies linearly between these values at intermediate temperatures. Processes in warm (liquid) and in ice clouds are therefore distinguished, but interactions between solid and liquid phases are not considered. We consider two classes of hydrometeors: droplets (and ice crystals) which are suspended in the cloud and whose size distribution is denoted $n(r)$ (m^{-4}), and raindrops which are falling through the atmosphere and whose size distribution is denoted $N(R)$ (m^{-4}). The cloud liquid water and the rainwater mixing ratios are found by summing the water contained in these two classes of particles, respectively.

Conversion of cloud liquid water to rainwater occurs through autoconversion of droplets to raindrops and collection of droplets by falling raindrops. Rain evaporates if it falls through subsaturated layers.

The continuity equations for the cloud water and the rainwater mixing ratios, q_l and q_r, are

$$\frac{\partial q_l}{\partial t} = C - f\,x\,(R_{ll}+R_{lr}) - (1-x)\,f\,R_i - \frac{1}{\rho_{\text{air}}}\text{div}(\boldsymbol{u}\,\rho_{\text{air}}\,q_l) \tag{1}$$

$$\frac{\partial q_r}{\partial t} = f\,x\,(R_{ll}+R_{lr}) - (1-f)\,E_r - \frac{1}{\rho_{\text{air}}}\left(\frac{\partial}{\partial z}(\rho_{\text{air}}\,V_r\,q_r) + \text{div}(\boldsymbol{u}\,\rho_{\text{air}}\,q_r)\right) \tag{2}$$

where C, R_{ll}, R_{lr}, R_i, and E_r are the rates (kilograms water per kilograms air per second) of condensation, autoconversion, collection, release of solid precipitation, and evaporation of falling raindrops, respectively. (See the notation list for other symbols).

In contrast to ice precipitation which is instantaneously removed from the atmosphere (see below), liquid precipitation (raindrops) remains stored in the atmosphere for a finite time period, during which the microphysical processes involving rainwater (such as the collection of droplets by falling raindrops or rainwater evaporation) can occur. We have chosen to time step the precipitation process and to solve the rainwater budget equation in prognostic form with a semi-implicit scheme. The time step required to accurately represent the microphysical processes (6 minutes here) is also appropriate for solution of the rainwater budget equation. This approach is in contrast to that of *Ghan and Easter* [1992] and *Ose* [1993] who computed the rainwater (as well as snow or graupel) mixing ratios diagnostically, but it is similar to the approach of *Fowler et al.* [1995].

The definition of R_i is identical in this version of the model to that in the standard version

$$R_i = \frac{1}{\rho_{\text{air}}}\frac{\partial}{\partial z}(\rho_{\text{air}}\,V_i\,l) \tag{3}$$

where l is the in-cloud cloud water content, and $V_i = 3.29\,(\rho_{\text{air}}\,l)^{0.16}$ (meters per second) is the mean terminal velocity for ice crystals calculated by *Heymsfield and Donner* [1990]. Equation (3) is based on the assumption that these solid hydrometeors immediately fall and reach their terminal velocity. We further assume that ice which is lost for each layer reaches the ground instantaneously. This assumption is certainly unrealistic in many respects, but a detailed treatment of ice clouds will be the subject of a further study. The solid precipitation flux (kilograms water per square meter per second) at the ground is then

$$P_i = \sum_{\text{layers}} f\,(1-x)\,\rho_{\text{air}}\,l\,V_i \tag{4}$$

P_l, is the flux of rainwater at the ground

$$P_l = \rho_{\text{air}}\,V_r(z=0)\,q_r(z=0) \tag{5}$$

so that the total precipitation flux at the ground is

$$P = P_l + P_i \tag{6}$$

We now describe our parameterization of the three main microphysical processes.

Autoconversion. This is the most important microphysical process since it initiates the precipitation. It is assumed that droplets fall relative to the air at their terminal velocities. The mass growth rate due to

collisions of a droplet with radius r and mass $m(r)$ is

$$\left(\frac{dm(r)}{dt}\right)_{\text{autoconversion}} = \int \pi(r+r')^2 \, |V(r) - V(r')| \, E(r,r') \, m(r') \, n(r') \, dr' \quad (7)$$

where $\int m(r')n(r')dr' = l \, \rho_{\text{air}}$. Only droplets with different sizes, and therefore different terminal velocities, can aggregate to form raindrops; otherwise the term $|V(r) - V(r')|$ in (7) vanishes. The integral in (7) must be approximated in the absence of droplet spectral information. We follow *Liou and Ou* [1989] and *Baker* [1993] in computing an upper bound to $dm(r)/dt$ by putting $r \gg r'$, $V(r') \equiv 0$, and $E(r,r') \equiv 1$. According to *Rogers and Yau* [1989], the terminal velocity of a droplet for $r \leq 20$ μm is given by $V(r) = k \, r^2$ with $k = 1.19 \, 10^8$ m^{-1}s^{-1}. We introduce a threshold value for r below which we assume autoconversion cannot occur (the collision efficiency is too small) and we multiply the resulting integral by a coefficient c smaller than unity to take into account the different approximations which were made. Our approximation for the autoconversion rate is then

$$R_{ll} = \pi \, c \, k \, l \, {r_4}^4 \, N \, H(r_4 - r_0) \quad (8)$$

where H is the Heaviside function. $N{r_n}^n = \int r^n n(r)dr$ is the n^{th} moment of the droplet radius distribution and $r_n = (\int r^n n(r)dr / \int n(r)dr)^{\frac{1}{n}}$ is the equivalent radius for the n^{th} moment of the size distribution. (For instance r_2 and r_3 are the surface-weighted and the volume-weighted mean radii of the size distribution, respectively.) *Liou and Ou* [1989] used (8) in a one-dimensional model but kept r_4 constant. However, it seems reasonable to relate r_4 and l. Integrating the droplet mass over the whole spectrum, we get the following equation

$${r_3}^3 = \frac{l \, \rho_{\text{air}}}{\frac{4}{3}\pi \, \rho_{\text{water}} \, N} \quad (9)$$

Here r_3 is a different measure of the size distribution than r_4 but these two quantities are strongly correlated for sufficiently narrow size distributions. Examination of aircraft data from trade and continental cumulus and marine stratocumulus [*Bower et al.*, 1994] suggests that all characteristic radii (i.e., r_2, r_3, r_4) are about the same for unglaciated clouds. The ratio r_4/r_3 is 1.03 ± 0.03 and can be higher (about 1.2) for trade cumulus and mixed liquid ice clouds (A. Blyth, personal communication, 1994). We adopt here a constant ratio of 1.1. In other terms, this means that we ignore the variations in the droplet spectral shape. This is a weakness of our scheme because the autoconversion rate is actually highly dependent on the presence of a few large droplets [*Beard and Ochs III*, 1993] but it would require too much complexity to compute a droplet size distribution. Finally, substituting (9) in (8), we have the following expression for the autoconversion rate:

$$R_{ll} = c' \, {\rho_{\text{air}}}^{\frac{4}{3}} \, l^{\frac{7}{3}} \, N^{-\frac{1}{3}} \, H(c'' \, l^{\frac{1}{3}} \, {\rho_{\text{air}}}^{\frac{1}{3}} \, N^{-\frac{1}{3}} - r_0) \quad (10)$$

where $c' = 1.1^4 \, (\frac{3}{4})^{\frac{4}{3}} \, \pi^{-\frac{1}{3}} \, {\rho_{\text{water}}}^{-\frac{4}{3}} \, c \, k$ and $c'' = 1.1 \, (\frac{3}{4})^{\frac{1}{3}} \, \pi^{-\frac{1}{3}} \, {\rho_{\text{water}}}^{-\frac{1}{3}}$. Equation (10) is close to the form used by *Chen and Cotton* [1987] but differs by the absence of their term involving spatial inhomogeneities in the liquid water content. In Figure 2 we show the autoconversion rate as a function of liquid water content for several values of the cloud droplet concentration N and for three values of the threshold radius r_0.

Collection. We now consider a raindrop with radius R and mass $M(R)$ collecting cloud droplets. Its mass growth rate is approximately:

$$\left(\frac{dM(R)}{dt}\right)_{\text{collection}} = \pi \, R^2 \, V(R) \, l \, \rho_{\text{air}} \quad (11)$$

We assume that $V(R) = k_2 (\frac{\rho_0}{\rho_{\text{air}}})^{\frac{1}{2}} R^{\frac{1}{2}}$, which is a good approximation if 600 μm $\leq R \leq$ 2000 μm. According to *Rogers and Yau* [1989], $k_2 = 2 \, 10^2$ m$^{\frac{1}{2}}$ s^{-1} and $\rho_0 = 1.2$ kg m^{-3}. Assuming a Marshall-Palmer distribution for the raindrop radius (i.e., $N(R) = N_0 \, e^{-R/R_m}$, *Marshall and Palmer* [1948]) and introducing

$$q_r = \frac{\rho_{\text{water}}}{\rho_{\text{air}}} \int \frac{4}{3}\pi R^3 N(R) dR, \quad (12)$$

we obtain after integration over R

$$R_{lr} = \frac{k_2 \Gamma(\frac{7}{2})}{8} \, \frac{{\rho_0}^{\frac{1}{2}} {\rho_{\text{air}}}^{\frac{1}{2}}}{\rho_{\text{water}}} {R_m}^{-\frac{1}{2}} \, l \, q_r \quad (13)$$

Note that the characteristic radius, R_m, is prescribed and is independent of q_r, unlike the parameterization of *Kessler* [1969]. Equation (13) is similar to that used in *Tripoli and Cotton* [1980].

Evaporation of raindrops. Evaporation of droplets is implicitly treated in the evaporation-condensation scheme, although crudely. That is why we only explicitly describe evaporation of raindrops which are falling in clear sky. For a raindrop with radius R,

$$\frac{dM(R)}{dt} = 4 \, \pi \alpha \, R \left(\frac{q_{\text{clear}}}{q_{\text{sat}}} - 1\right) \quad (14)$$

where α=1.05 10^{-6} kg m^{-1} s^{-1} [*Liu and Orville*, 1969]. If we proceed as previously, then the evaporation rate of rainwater is

$$E_r = -\frac{\alpha}{2} \left(\frac{q_{\text{clear}}}{q_{\text{sat}}} - 1\right) \frac{q_r}{\rho_{\text{water}} \, {R_m}^2} \quad (15)$$

Sundqvist [1988] and *Schlesinger et al.* [1988] expressed the evaporation rate as a function of the precipitation rate rather than the rainwater content, which was not explicitly calculated in their scheme. Our equation is similar to that of *Kessler* [1969] but differs in the exponent of rainwater content.

In the derivation of the collection and rainfall evaporation rates, we made the assumption of a random vertical overlapping of the cloud layers, which is reasonable here in view of the low vertical resolution. Raindrops from a given layer fall equally in the cloudy and clear sky parts of the underneath layer.

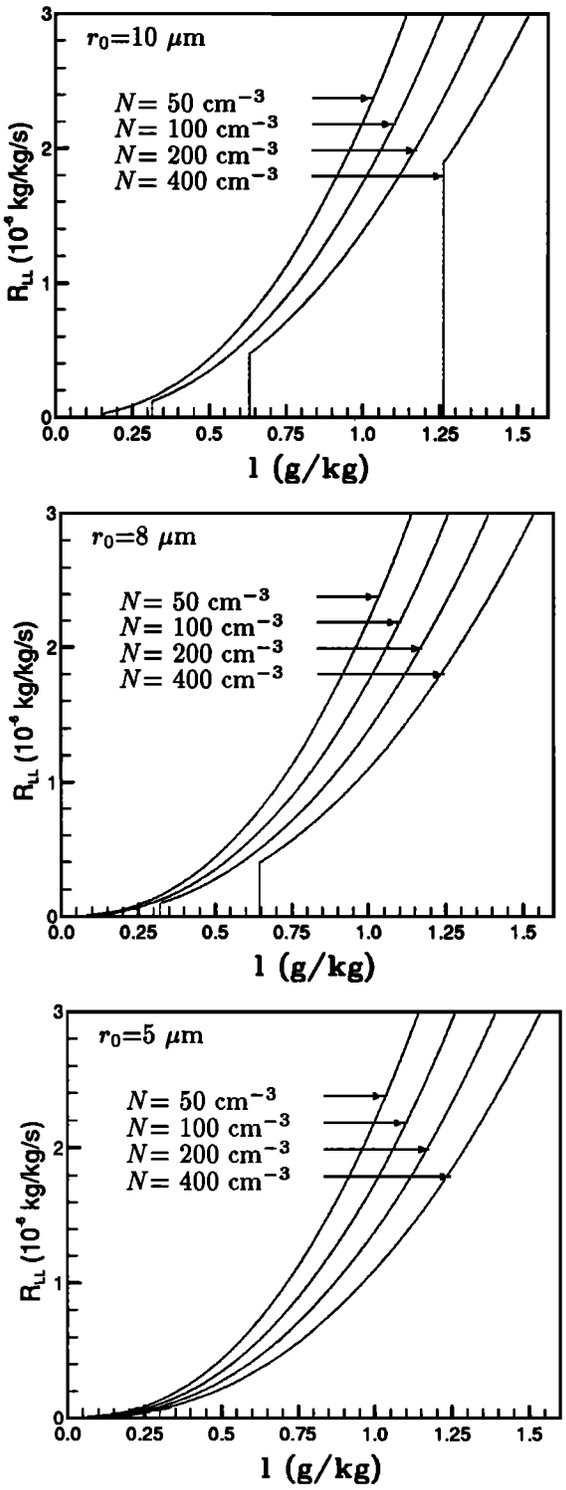

Figure 2. Autoconversion rate, R_{ll} (10^{-6} kg/kg s^{-1}), as a function of the in-cloud liquid water content, l (g/kg).

The determination of some parameters introduced here (R_m, c, r_0, N) is essential since these will control the fraction of cloud water which remains stored in the atmosphere. These parameters vary with the type of clouds, but cloud microphysical observations can provide us with typical values. The multiplicative coefficient c (as in (8)) is difficult to assess theoretically but data from maritime cumulus and stratocumulus show a value ranging between 0.01 and 0.1 [*Baker*, 1993]. However, better results, in terms of climate statistics, are obtained in our model if c is set to larger values. For these reasons, we use $c = 1$ here. There exist some physical explanations for this discrepancy. The highly nonlinear dependence of the autoconversion rate on l (as in (10)) results in an underestimation of the autoconversion rate if the rate is predicted from a single value (i.e., the grid box average) of the in-cloud liquid water content. Also the large vertical extent of our clouds (which must fill a whole layer in the vertical) lowers the liquid water content. For these reasons, the direct introduction into a GCM of a scheme tuned with point observations may lead to systematic errors in model results.

In section 4, we will make detailed tests of the sensitivity of the parameterization to two parameters: the threshold radius r_0 (as in (10)) and the cloud droplet concentration N. This is motivated by the fact that the results are quite sensitive to both parameters. Whereas r_0 is an "internal" parameter of our parameterization, N is controlled by external parameters (concentration of cloud condensation nuclei (CCN) for instance) and can vary for identifiable reasons.

4. Results

We now present results from a one-dimensional model and a GCM, both based on our parameterizations of the microphysical processes. In this section, the cloud optical properties depend on the simulated cloud fraction and cloud water content but not on the mean cloud droplet radius, the value of which is being prescribed.

4.1. Results From a One-Dimensional Climate Model

For a preliminary evaluation of the model formulation we use a one-dimensional equilibrium model which is more convenient to handle than the full model. This allows us to study the effects of microphysical processes on the various cloud variables, level by level, without interference from the model dynamics which would add variability to the model results. This model, described in *Li and Le Treut* [1990], is a column climate model with parameterizations of diffusion, convection, and radiation that follow those of the GCM. It has no lateral boundary conditions and the only input parameters are the zenith angle of incident radiation, the length of day, the surface albedo, and the adjustable parameters of the different parameterizations. The model has been modified by the introduction of the microphysical scheme presented here (as in (1)–(15)), which is the same as

that in the GCM. After a 3-year integration, the model climate reaches an equilibrium state which depends on the boundary conditions and prescribed parameters but not on the initial state. The relative importance of the different microphysical processes can be assessed from Figure 3. Ice precipitation is the dominant process down to level 5 (where the transition between liquid and ice clouds occurs). Autoconversion is the dominant process for warm clouds whereas collection is also important but occurs at lower levels where the rainwater content is larger. It is worth noting that the autoconversion rate is high even at levels where collection occurs because our bulk parameterization of the microphysical processes does not represent the autoconversion cutoff which occurs when falling drops sweep small and medium-sized droplets efficiently. Evaporation of rainfall is here of secondary importance.

Experiments were made to investigate the sensitivity of the model results to various parameters. Experiments in which the characteristic raindrop radius, R_m, is varied show that the mean atmospheric state is not sensitive to R_m. The precipitation rate increases by only 1% if R_m is increased from 100 to 1000 μm. This can be explained by the low rates of collection and rainfall evaporation and by the low dependence of R_{lr} on R_m. R_m is therefore set to 1000 μm in the rest of the study. However, our results are sensitive to both the threshold radius, r_0, and the cloud droplet concentration, N. As can be seen from Figure 2, the effect of an increase in the threshold radius is to truncate the curve of the autoconversion rate versus l and to delay the release of precipitation. (A twofold increase in r_0 requires an eightfold increase in l before precipitation starts but precipitation above this cutoff is then very strong.) There are two effects of an increase in the cloud droplet concentration: first, it modifies the onset of the precipitation (a twofold increase in N requires a twofold increase in l for precipitation to begin) and second, it diminishes the autoconversion rate (by a factor of about 5 for a same twofold increase in N). Collection is also indirectly affected by changes in N and r_0. Our results are more sensitive to r_0 than to N but the range of variation is smaller: r_0 is in the range of 5 to 10 μm whereas N can vary over a very large range.

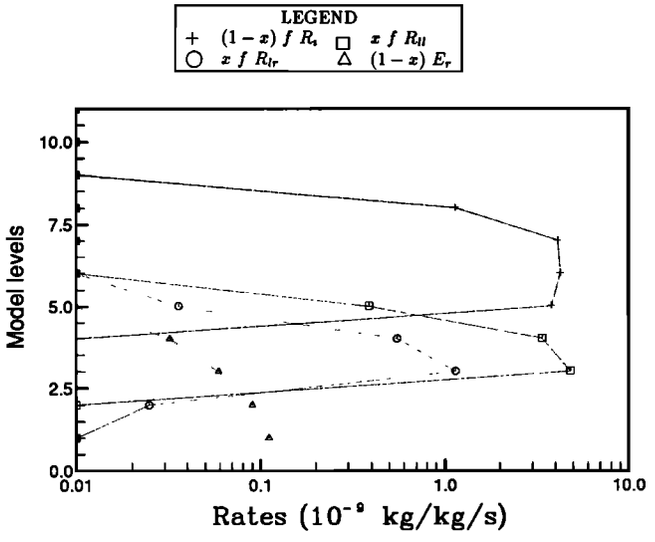

Figure 3. Rates of the different cloud microphysical processes.

Table 1 summarizes the values of input and output parameters of the one-dimensional model for a set of three experiments having different (r_0, N) values. The output parameters are the values obtained at equilibrium. In Figure 4 we further represent the vertical profiles of the mean volume droplet radius, the in-cloud cloud water content, and cloudiness. N is first increased from 50 to 200 cm^{-3} and r_0 is set to 5 μm. As can be seen from Figure 2, this change mostly affects the magnitude of the autoconversion rate but does not modify its onset much, which occurs at low liquid water content. The cloud fraction and the in-cloud cloud water content always vary in phase with N, but the mean droplet radius variations are negatively correlated with variations in N; this is consistent with the fact that increasing N leads both to a decrease in the mean droplet radius and a less efficient precipitation process as shown in (9) and (10). In order to isolate the increase in l from the increase in f, we have prescribed the vertical distribution of cloudiness in the model at its equilibrium value in the (r_0 = 5 μm, N = 50 cm^{-3}) run and set N to 200 cm^{-3}. The model climate then adjusts itself to a new liquid water content, which is about the same as in the case where f varies freely. This tends to prove that the autoconversion rate determines the liquid water content, which in turn determines cloudiness through the stratiform condensation scheme described in section 2.

These results are, to some extent, supported by in situ measurements of liquid water content and cloud droplet radii in ship tracks [*King et al.*, 1993]. It is reported that liquid water content is significantly enhanced in the ship track regions while cloud droplet radii decrease and the droplet concentration increases by a factor of 2 or so.

In a third experiment, r_0 is doubled while N is fixed at a value (200 cm^{-3}) which ensures a relative strong dependence of the switch on r_0 (Figure 2). The sensitivity of the cloud fraction and cloud water content to r_0 is very high. However, the mean volume droplet radius is much less sensitive to r_0. This is because l varies as the cube of r_3.

4.2. Results From a GCM

Here r_0 is set to 5 μm and N to 100 cm^{-3} for maritime clouds and 400 cm^{-3} for continental clouds. These values are within the range of observation [*Bower et al.*, 1992]. The model is integrated under January and July conditions. The mean precipitation field is shown on Figure 5. The mean monthly values of the precipitation rate for January are 2.31 and 2.91 mm d^{-1} in the northern hemisphere and the southern hemisphere, respectively. For July, these values are 2.89 and 2.36 mm d^{-1}, respectively. The precipitation pattern simu-

Table 1. Inputs and Outputs of the One-Dimensional Model

Experiment	Input Parameters					Output Parameters at Equilibrium				
	Zenith Angle	Fraction of Day	Surface Albedo	r_0	N	Surface Fluxes SW	Surface Fluxes LW	Planetary Albedo	Surface Temperature	Rain
A	60°	0.5	0.16	5	50	179.4	97.5	0.291	289.6	2.46
B	60°	0.5	0.16	5	200	177.1	96 2	0.298	289.4	2.43
C	60°	0.5	0.16	10	200	165.4	95.1	0 337	285.3	1.91

Fluxes are in watts per square meter. Temperature is in K. Also, r_0 is threshold cloud droplet radius in micrometers. N is cloud droplet number concentration in cubic centimeters. Rain is measured in millimeters per day.

lated by the GCM is very plausible, with good correspondence of the maxima with the observed values of *Jaeger* [1976] or *Legates and Willmott* [1990]. In zonal mean the correspondence is also good, with a discrepancy in the southern hemisphere which is common to many models [International Panel on Climate Control (IPCC), 1990]. This is not proof that our microphysical model is correct, because the difference between the two model versions with and without microphysics is small (see Figures 5a and 5b). This difference is smaller than the rms of the precipitation field, if we make five independent experiments by choosing five different initial January 1 states. On a monthly mean basis the large-scale precipitation pattern appears to be essentially a reflection of the large-scale convergence of the water vapor and is little affected by cloud microphysics. This is because the atmospheric reservoir of cloud water remains small compared to that of water vapor.

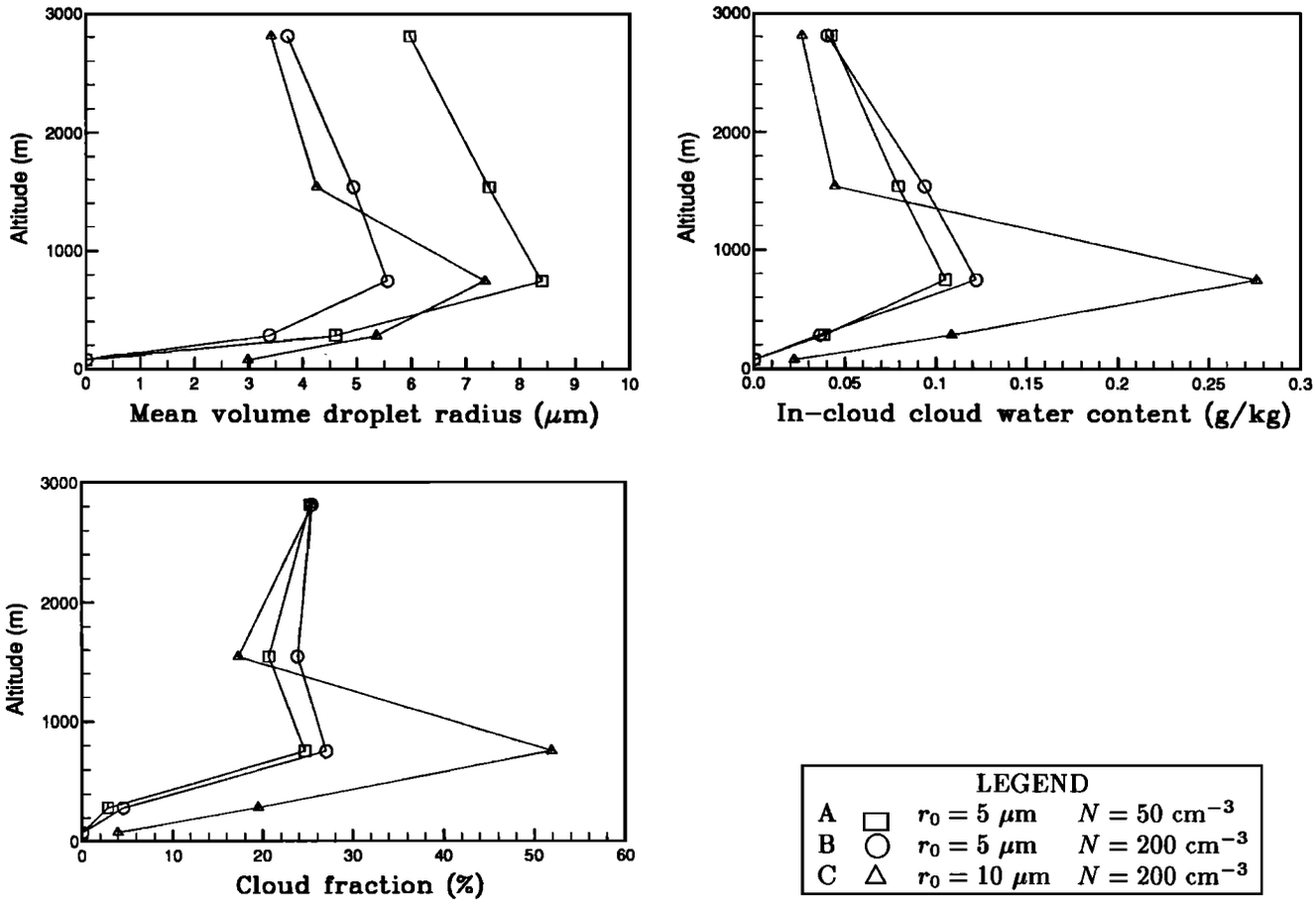

Figure 4. Vertical profiles of the mean droplet radius, in-cloud cloud water mixing ratio, and cloud fraction in a one-dimensional model for different values of r_0 and N.

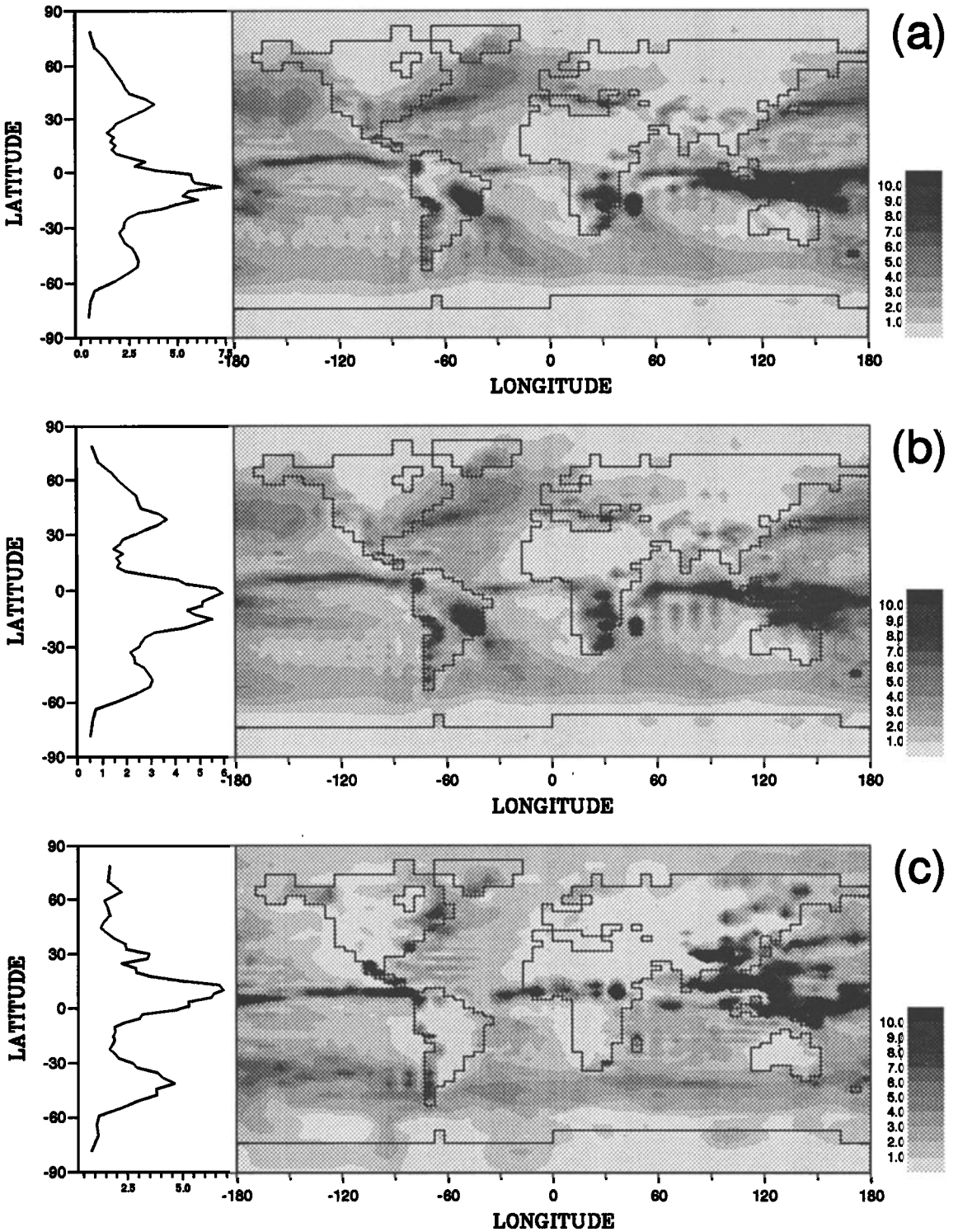

Figure 5. Precipitation rate (millimeters per day): (a) January simulation including cloud microphysics (average on five simulations), (b) January simulation using the control version of the model, (c) July simulation including cloud microphysics.

The zonal profiles of relative humidity and cloud water mixing ratio are plotted in Figures 6 and 7. The distribution of relative humidity is very similar to that of the standard version of the model, run in the same conditions. The zonal profiles of the cloud water mixing ratio in this version of the model and in the standard version are qualitatively similar but values are higher in this version. Zonal profiles of cloud volume fraction are plotted in Figure 8. There are typically two levels of clouds, which form where relative humidity is highest, especially in the low troposphere. Also shown in Figure 9 is the mean volume droplet radius, r_3, at the

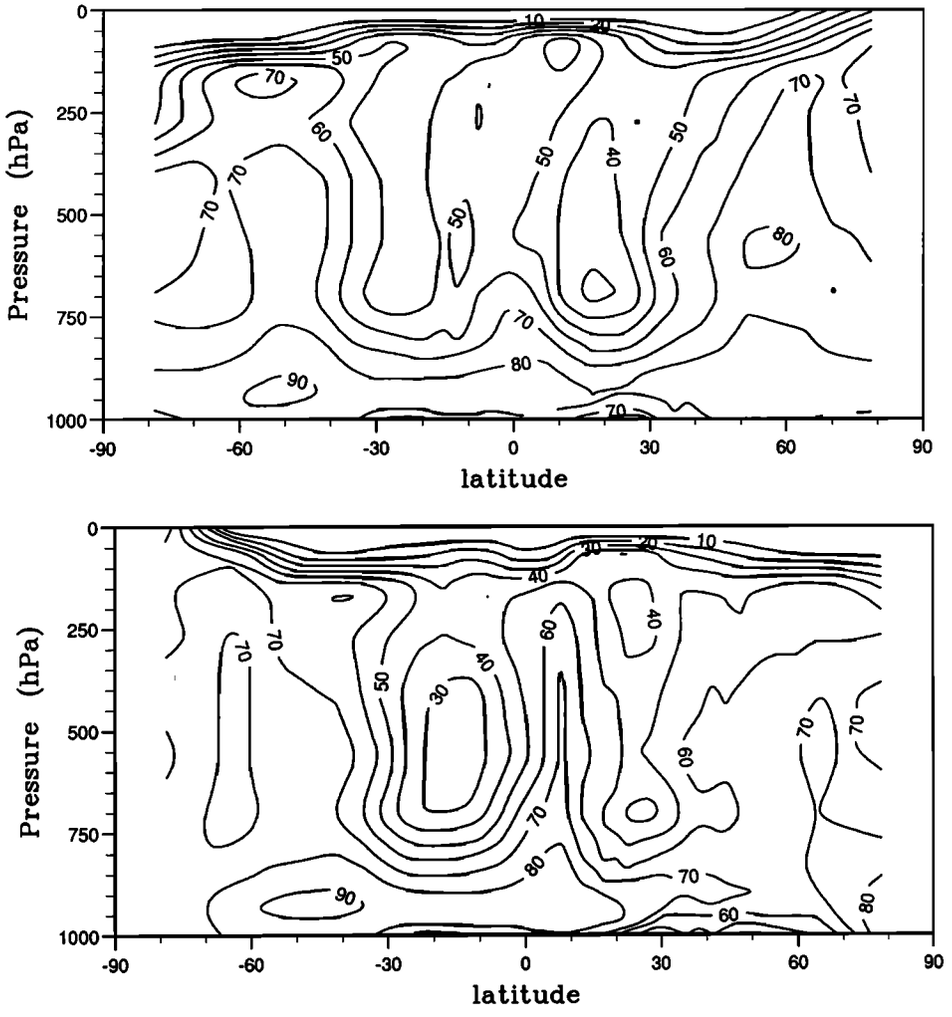

Figure 6. Latitude-altitude cross section of relative humidity for a month of (a) January, and (b) July. Contour interval is 10%.

second level ($\approx$ 950 hPa) of the model for a month of January. Radii are much larger over the ocean than over land. This can be explained by the fact that cloud droplet concentration is prescribed at a higher value over land but also because there is less water available over some land areas, due to lower surface evaporation. This point will be discussed below. The vertically integrated cloud liquid water content (precipitable liquid water) is shown in Figure 10. The geographical distribution of this quantity is fairly realistic with maxima along the Intertropical Convergence Zone (ITCZ) and over the oceans in the extratropics. The simulated magnitude is also in good agreement with special sensor microwave imager (SSM/I) data.

We made two series of sensitivity experiments (see Table 2 for a list of experiments)in order to explore the dependence of the results on the model assumptions. All the sensitivity experiments are run under January conditions.

Sensitivity to r_0. Two experiments (R1 and R2) were performed with r_0 set to 5 and 10 μm, respectively. N is set to 50 cm^{-3} for maritime clouds and 200 cm^{-3} for continental clouds. Figure 11 represents the zonal profile of the difference of cloud water mixing ratio between the two sensitivity experiments (R2–R1). Positive values show a larger cloud water mixing ratio in the lower troposphere if $r_0 = 10$ μm. The increase is about 50% on the average but reaches 100% at some locations. Concomitantly, the mean droplet radius is increased by about 0.5 μm with a larger increase over continents because of the larger dependence of the autoconversion rate on r_0 at high cloud droplet concentration (see Figure 12). The cloud cover (computed assuming a maximum/random overlapping [*Sundqvist et al.*, 1989]) is increased from 56.7% to 59.5% on global average. As far as global averages of cloud water content, cloudiness and droplet radius are concerned, the model responses are very similar to those of the one-dimensional model. We also observe a general cooling of the atmosphere at low and midlatitudes associated with the increase in cloud optical thickness. This is accompanied by a warming at high latitudes (Figure 13). This behavior is reminiscent of that obtained by *Kiehl* [1994], when he decreased cloud droplet effective radius over land, producing, as in our case, a larger cloud

albedo effect. The temperature changes are stronger over land because, sea surface temperatures (SSTs) being fixed, the ocean acts as a heat source (or sink) of infinite capacity. The equator-to-pole gradient of temperature is decreased in R2 compared to R1 and the winter Hadley cell is significantly weakened (Figure 14). The meridional circulation is hardly changed at other latitudes.

We believe that r_0=5 μm is more appropriate here although the collision efficiencies are very low for droplets with radius below 5 μm. What is actually described in the partial cloud cover parameter, f, is a set of clouds, some of which are precipitating and some of which are not. Obviously, some of the clouds will precipitate before the threshold radius is reached for the whole set of clouds. It is therefore legitimate to use a smaller threshold radius than that suggested by the dependence of collision efficiencies on droplet radii.

Sensitivity to N. Here r_0 is fixed and N is the same for all clouds: 50 cm^{-3} in the first experiment (N1) and 200 cm^{-3} in the second one (N2). Again, we look at the zonal profile of the difference of cloud water mixing ratio between the two sensitivity experiments (N2–N1) (see Figure 15). The cloud water mixing ratio is larger in the troposphere in the case N=200 cm^{-3}. Globally (i.e., vertically and horizontally) averaged, the increase in cloud water between experiments N1 and N2 is 10%. This is consistent with (10), which shows that the autoconversion rate decreases with increasing N, all other parameters being held constant. Moreover, if N is increased, the mean radius is reduced and is less likely to reach the threshold value. It is also remarkable that on the average, the product $l^{\frac{7}{3}} N^{-\frac{1}{3}}$, which is proportional to the autoconversion rate, remains constant when N is increased. The climate system responds to the perturbation in N in such a way that the overall amount of precipitation remains constant. The cloud cover is also affected by the change in N but to a lower extent: its value is 56.4% and 57.4% in experiments N1 and N2, respectively. The increase in cloud cover is mostly a consequence of increased cloud volume fraction in the lower layers (1000–800 hPa). However, the water vapor content remains almost unchanged in the two experiments: we only observe a 0.5% increase in the precipitable water (vertically integrated water vapor) between the two experiments. Figure 16 shows the mean change in low cloud droplet volume radius between experiments

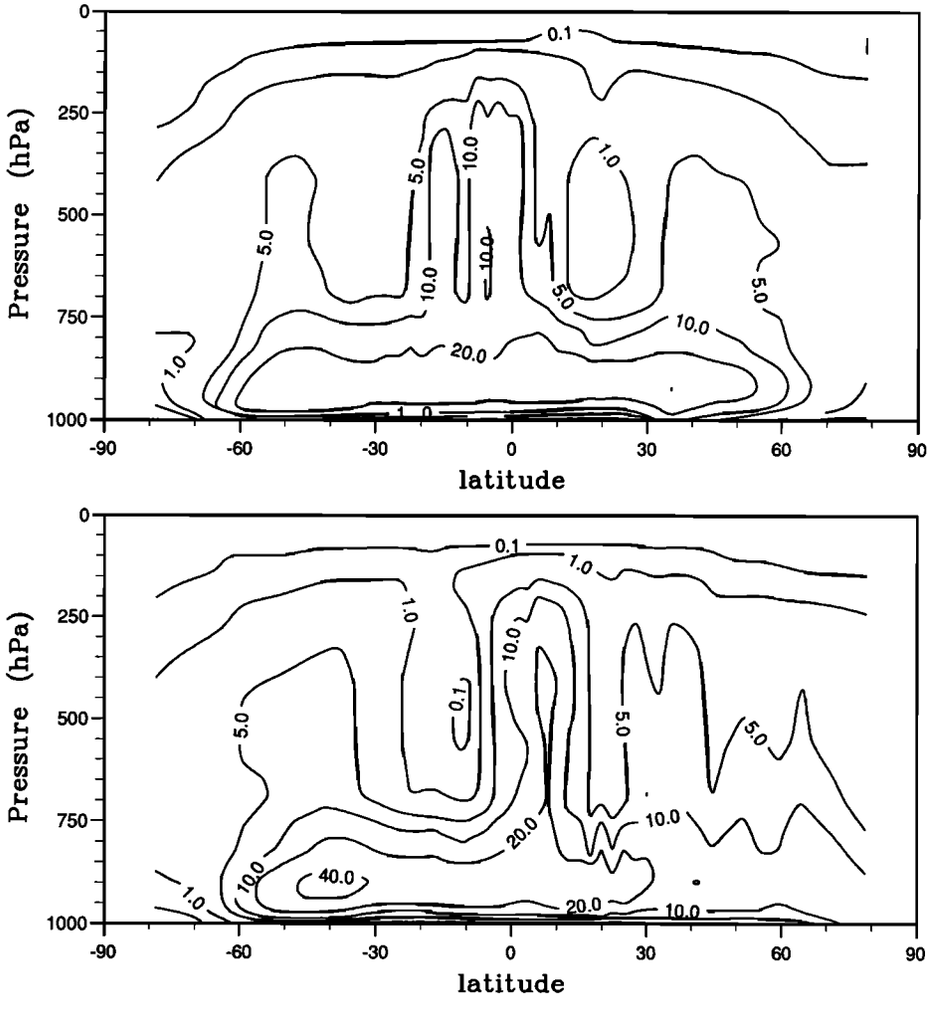

Figure 7. Latitude-altitude cross section of grid box average of cloud liquid water for a month of (a) January, and (b) July. Isolines are 0.1, 1, 5, 10, 20, and 40 mg/kg.

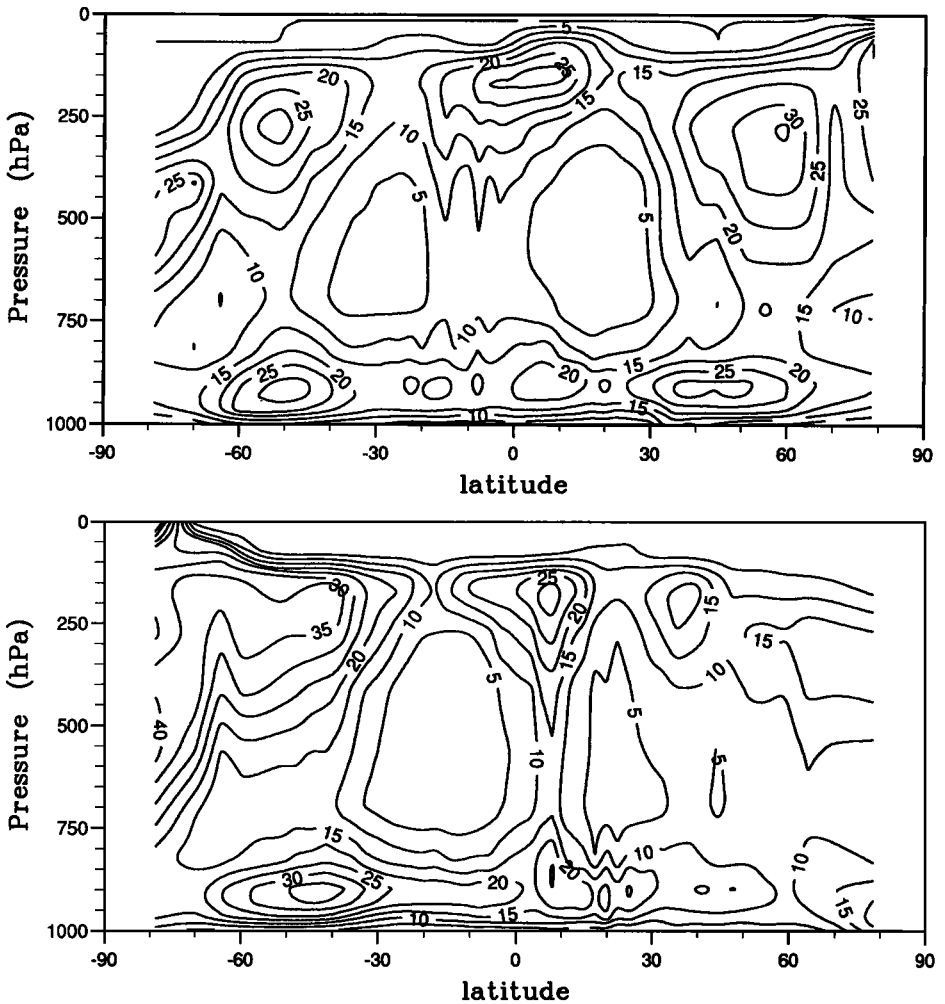

Figure 8. Latitude-altitude cross section of cloud volume fraction for a month of (a) January, and (b) July. Contour interval is 5%.

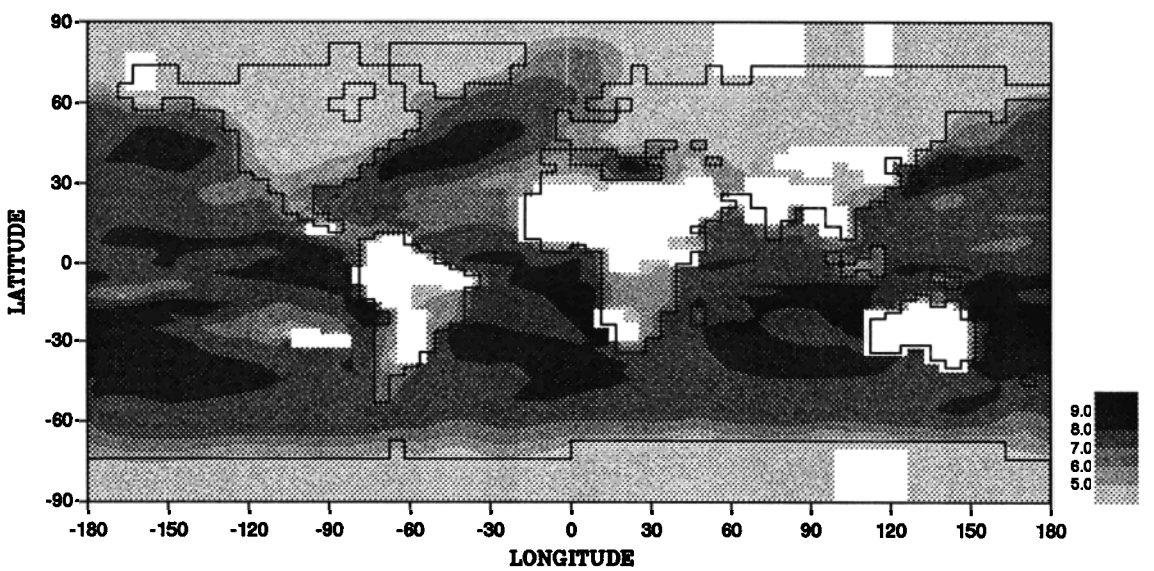

Figure 9. Mean volume droplet radius (micrometers) as simulated by the model at level two ($\approx$ 950 hPa) under January conditions.

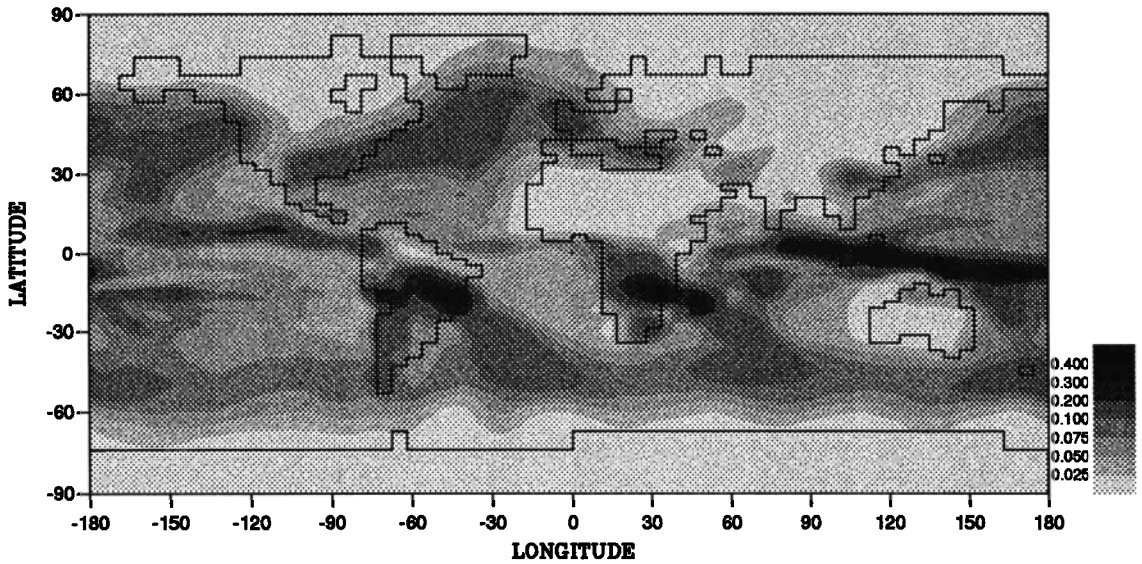

Figure 10. Vertically integrated cloud water (kilograms per square meter) as simulated by the model under January conditions.

N1 and N2 . There is a general decrease in r_3 over the globe. On the average, the difference in droplet radius is 3-4 μm, depending on the layers. The mean droplet radius in both experiments N1 and N2 is also smaller over land than over the ocean. Since cloud droplet concentrations are the same for the two types of clouds, this supports the idea that cloud droplet radius is not only dependent on N but also on the quantity of water vapor that is available.

We see in Figure 17 that the changes in atmospheric temperature are somewhat weaker than in the previous sensitivity experiments. Figure 17 also exhibits a more erratic structure, with largest changes at high latitudes. This behavior is consistent with the conventional picture of a higher climate sensitivity at high latitudes.

Table 2. List of Experiments

Experiment	r_0	N		r_w
		Ocean	Land	
Control	5	100	400	prescribed
R 1	5	50	200	prescribed
R 2	10	50	200	prescribed
N 1	5	50	50	prescribed
N 2	5	200	200	prescribed
IN 1	5	50	50	calculated
IN 2	5	200	200	calculated

Here r_0 is the threshold cloud droplet radius in micrometers. N is the cloud droplet number concentration in cubic centimeters. The effective radius for warm clouds, r_w, is either prescribed to a fixed value or calculated, as discussed in the text.

Note that the mean monthly hemispheric values of the precipitation rate are relatively constant in all cases, varying by less than 10%. This suggests again that the total amount of precipitation is first governed by the large-scale convergence of moisture and not by the microphysical processes.

5. Influence of the Cloud Droplet Concentration on Cloud Optical Properties

In this section the parameterization of the cloud optical depth is treated in a way that is consistent with the precipitation parameterization. The aim is not to get a more realistic model in terms of radiative fluxes, because it is obviously easier to prescribe the cloud droplet radius and use it as a tunable parameter than to compute it, but to introduce a potential new feedback which may be important for various types of climate change scenarios. We now explore the sensitivity of the new model to the cloud droplet concentration.

The equation used for the cloud optical depth in earlier sections was

$$\tau = \frac{3}{2}\frac{W}{\rho_{\text{water}}\, r_e} = \frac{3}{2}\frac{W}{\rho_{\text{water}}(x r_w + (1-x) r_c)} \qquad (16)$$

where W is the liquid water path, and r_e is the droplet effective radius (i.e., the ratio of the third moment to the second moment of the size distribution). Here r_e was approximated by a linear function of r_c and r_w, the effective radii for ice and warm clouds, respectively, which were prescribed to be 25 μm and 10 μm, respectively [*Stephens*, 1978; 1984]. Ice cloud effective droplet radius is larger in order to take into account the nonspherical shape of ice particles. The value of r_e is often chosen to tune the shortwave radiative fluxes simulated by the GCMs by comparison to the observed data. This

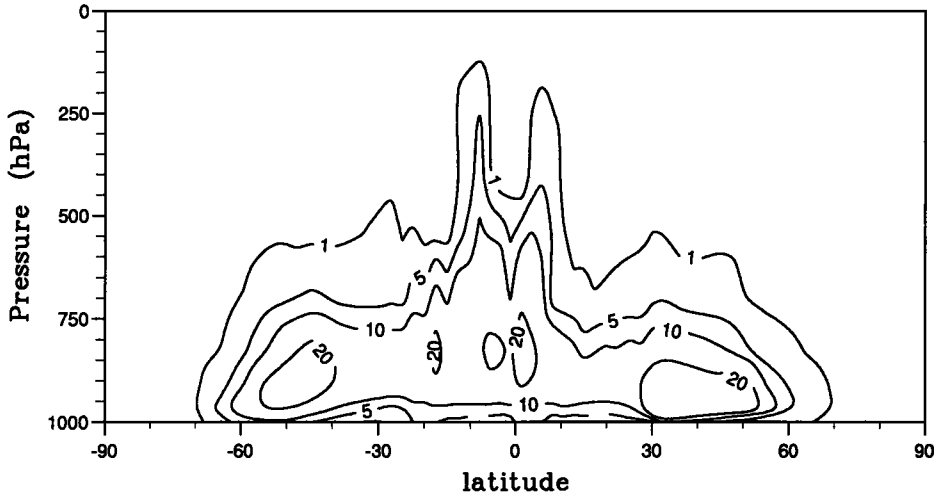

Figure 11. Difference map for the cloud water mixing ratio between the two sensitivity experiments (R2−R1). Isolines are -1, 0, 1, 5, 10, and 20 mg/kg.

is not satisfying since the only feedback on cloud optical depth which is allowed is then through the cloud water amount, whereas results are potentially sensitive also to changes in the value of r_e [*Charlock and Ramanathan*, 1985; *Slingo*, 1990]. From now on, we calculate r_e rather than prescribe it. The cloud optical depth is the sum of optical depths for warm and cold clouds, weighted by x and $(1-x)$, respectively [*Sun and Shine*, 1994].

$$\tau = x\,\tau_w + (1-x)\,\tau_c = \frac{3}{2}\frac{W}{\rho_{\text{water}}}\left(\frac{x}{r_w} + \frac{(1-x)}{r_c}\right) \quad (17)$$

which allows us to define an equivalent effective radius

$$r_e = \frac{1}{\frac{x}{r_w} + \frac{(1-x)}{r_c}} \quad (18)$$

The droplet effective radius for warm clouds, r_w, is calculated from the mean volume radius. We assume therefore a proportional relation between r_3 and r_2 (namely $r_3 = 1.1\ r_2$) giving $r_w = 1.21\ r_3$. This is consistent with measurements from *Martin et al.* [1994] who found a proportionality coefficient between mean volume and effective radii in stratocumulus clouds although their ratio, r_w/r_3, is different for continental (1.14) and maritime (1.08) air masses. The droplet effective radius for cold clouds, r_c, is set to its previous value (25 μm). In the case of a warm cloud ($x = 1$), (17) can be written as follows:

$$\tau = C\ h\ l^{\frac{2}{3}}\ N^{\frac{1}{3}} \quad (19)$$

where C is a constant and h the cloud thickness. This

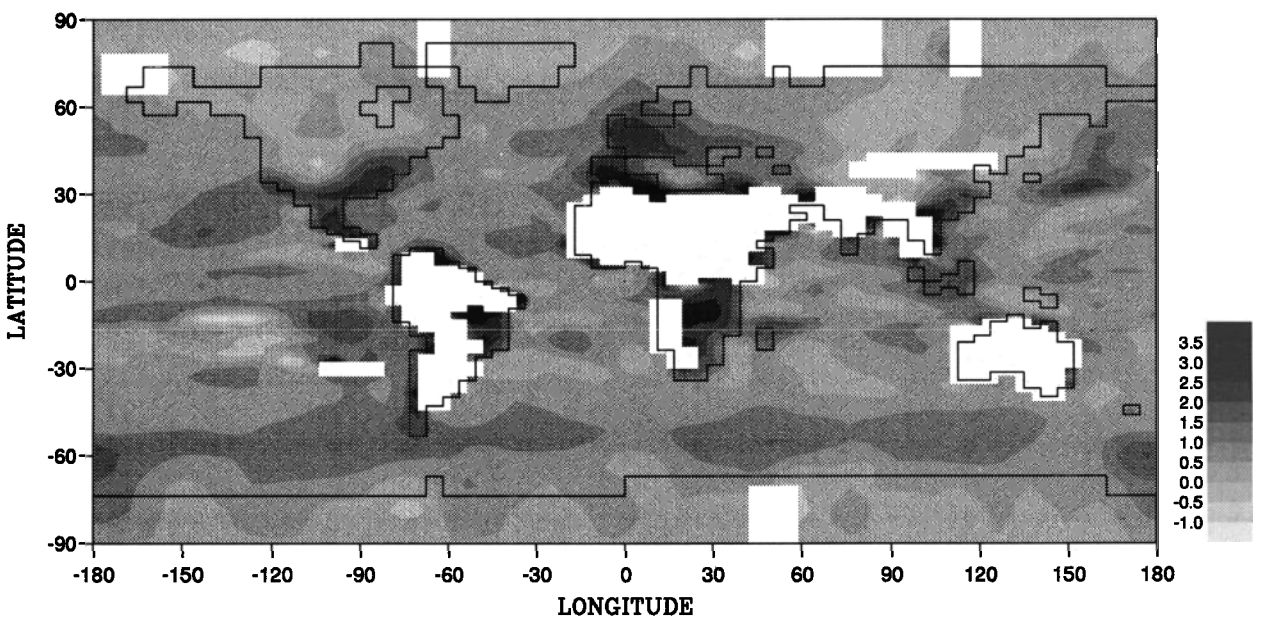

Figure 12. Difference (R2−R1) in mean volume droplet radius (micrometers).

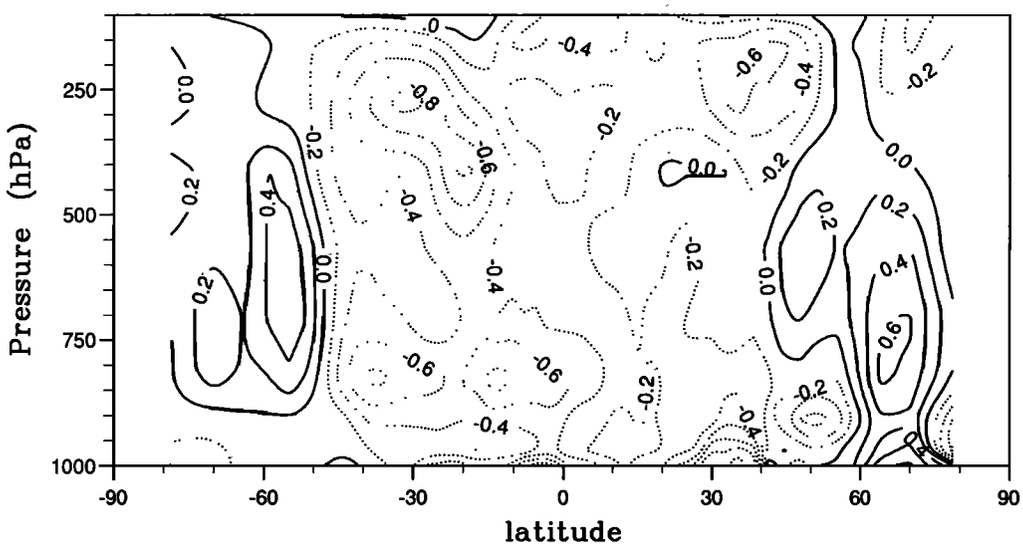

Figure 13. Difference map (R2–R1) for the zonally averaged temperature (K).

equation is similar to that proposed by *Bohren* [1985] and *Charlson et al.* [1992] but the dependence on N is stronger than it may appear because the cloud water mixing ratio increases with N. This effect was not taken into account in many of the previous studies [*Charlson et al.*, 1987; 1992; *Ghan et al.*, 1990] where l is held constant.

Again, we made several experiments with different values of N. To evaluate the results, we use the notion of cloud radiative forcing (CRF). It is defined as the difference between total and clear sky fluxes at the top of the atmosphere and can be divided into a shortwave (SW) and a longwave (LW) component:

$$CRF = CRF_{SW} + CRF_{LW} \quad (20a)$$

$$= S(\alpha_{\text{clear}} - \alpha) + (F_{\text{clear}} - F) \quad (20b)$$

where S is the insolation, α is the planetary albedo, and F is the outgoing longwave radiation; the index clear refers to clear sky conditions [*Ramanathan et al.*, 1989]. In the model, clear sky fluxes are computed separately at each grid point (which may be free from clouds or partly cloudy) and therefore correspond to combined clear/cloudy atmospheric conditions. This method, which is referred to as method II in *Cess and Potter* [1987], gives satisfactory results and is much more convenient than method I to implement in a GCM.

Sensitivity to N. Two more sensitivity experiments are performed with r_0 equal to 5 μm. N is equal to 50 cm^{-3} for all clouds in the first experiment (IN1) and to 200 cm^{-3} in the second experiment (IN2). This allows comparison with experiments N1 and N2. Changes in mean cloud droplet radii, cloud liquid water content and cloud cover due to this fourfold increase in N are very similar to those discussed in the previous section

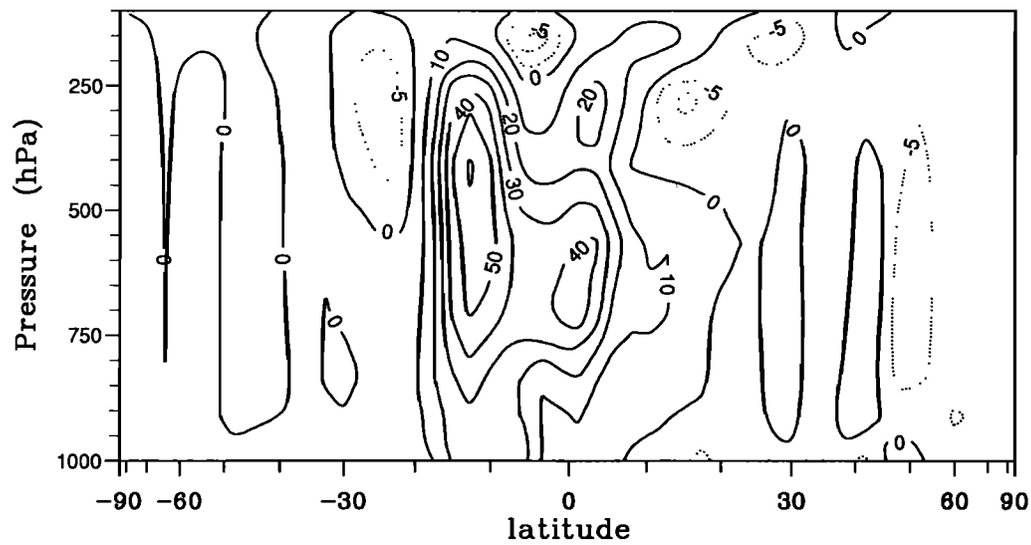

Figure 14. Change in mean meridional stream function (10^9 kg s^{-1}) due to prescribing a higher threshold radius for the precipitation onset (R2–R1).

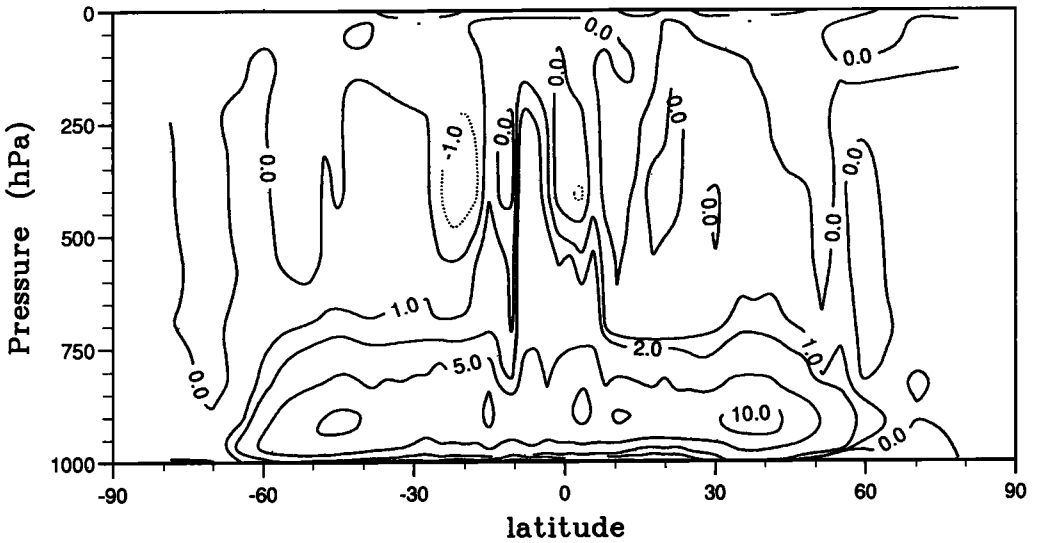

Figure 15. Difference map for the cloud water mixing ratio between the two sensitivity experiments (N2−N1). Isolines are -1, 0, 1, 2, 5, and 10 mg/kg.

(experiments N1 and N2). Changes in the zonally averaged air temperature (Figure 18) are comparable in magnitude to the changes obtained in the N1/N2 experiments. The zonal mean of the SW cloud radiative forcing is shown in Figure 19b. Comparison of the model results to Earth Radiation Budget Experiment (ERBE) observations shows that the model reproduces the shape of the latitudinal variation of cloud forcing fairly well. However, the minimum of the forcing is shifted towards the equator, which mostly is a consequence of the displacement of the minimum in surface pressure in the model and partly a consequence of the treatment of ice; our ice clouds are too thin at high latitudes. The forcing is also too high in the tropics. The fourfold increase in N induces a 14.3 W m^{-2} increase in the globally averaged SW CRF (from −50.9 to −65.2 W m^{-2}). Different reasons explain this important change: the decrease in cloud droplet radii, the increase in cloud water content, and cloudiness. A comparison with experiments N1 and N2 (Figure 19a) shows that this increase is not so large if the effective droplet radius is fixed: the forcing is enhanced by 7.1 W m^{-2} (from −50.6 to −57.7 W m^{-2}). Since the two series of sensitivity experiments (N1, N2 and IN1, IN2) only differ in the treatment of the effective radius in the computation of the cloud optical depth and because the integration time is short so that no secondary feedbacks are expected, the difference between the two changes in SW CRF (i.e., about 7 W m^{-2}) is a good approximation of the effect of the cloud droplet effective radius on the SW CRF. We therefore conclude that about half of the extra SW CRF forcing induced by the fourfold increase in N is due to change in cloud droplet radii, and the other half to changes in cloud water content and cloudiness.

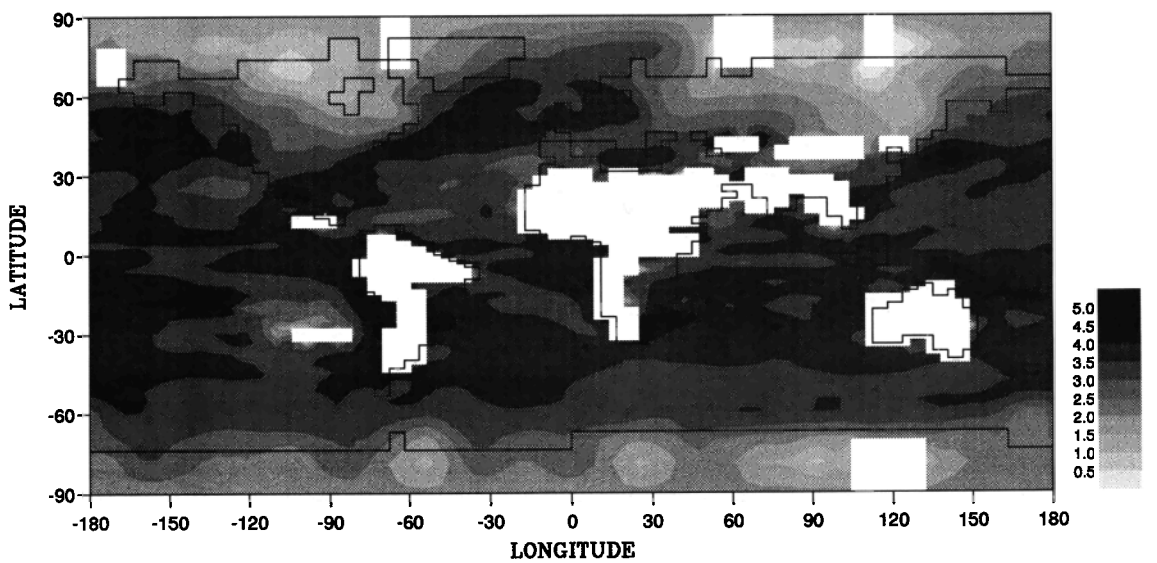

Figure 16. Change (N1−N2) in mean volume droplet radius (micrometers).

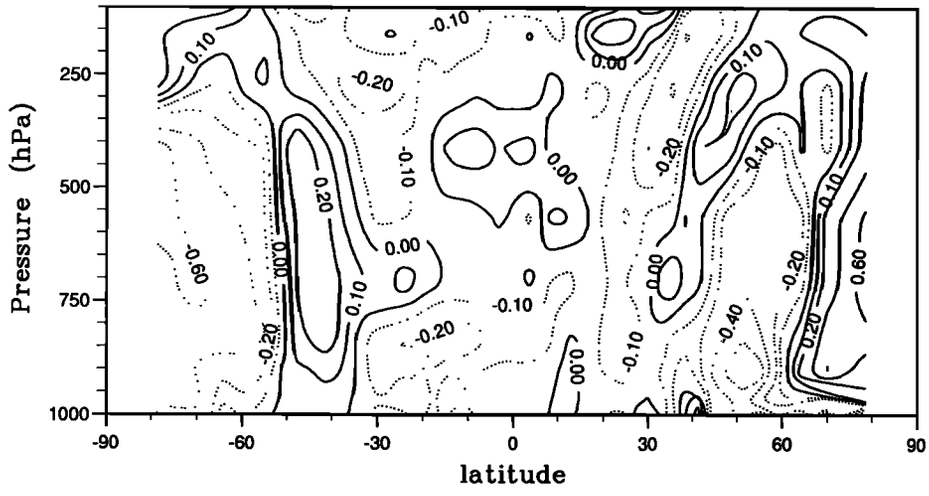

Figure 17. Difference map (N2–N1) for the zonally averaged temperature (K).

The LW CRF remains almost unchanged (see Figure 20) since it is mainly high clouds which influence the LW CRF, and they are unchanged by the parameterization introduced in the present study, when N is modified.

This sensitivity to N is larger than that inferred by *Ghan et al.* [1990] who found a global net radiative forcing of -6 W m^{-2} in response to a fourfold increase of maritime cloud droplet concentration (from 50 to 200 cm^{-3}). Note also that in our model, sea surface temperatures were prescribed, which tends to limit the climatic response. Nevertheless, our forcing may be consistent with Ghan et al. because in their study the precipitation rate does not depend on the cloud droplet number concentration. We estimate the effect of the cloud droplet effective radius on the SW CRF as the difference (IN2–IN1)–(N2–N1). This difference is -7 W m^{-2} and corresponds better to that computed by Ghan et al.

6. Summary and Conclusion

We have developed a parameterization of the precipitation rate which describes the cloud microphysical processes responsible for the production of warm rain. This parameterization is introduced in the LMD GCM and replaces the simple algorithms which were used previously. The cloud droplet concentration is prescribed and the mean cloud droplet radius is explicitly computed in this scheme. A cloud precipitates if the mean droplet radius is larger than a prescribed threshold radius, r_0. We have investigated the sensitivity of the model to several microphysical parameters. The results are quite sensitive to the threshold radius, r_0. The value of this parameter is uncertain and there is a need for measurements to allow its calibration. A high threshold radius significantly increases the amount of cloud water stored in the atmosphere. The results are also sensitive to the cloud droplet concentration, N. We have

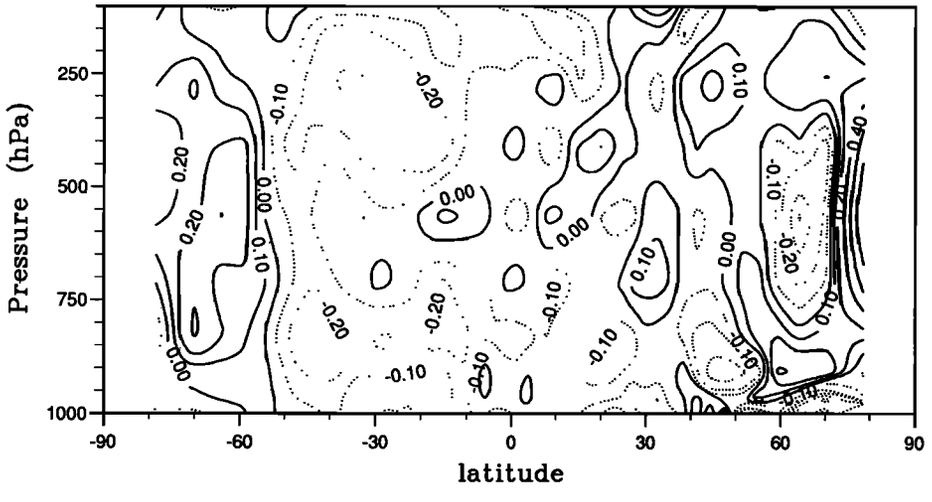

Figure 18. Difference map (IN2–IN1) for the zonally averaged temperature (K).

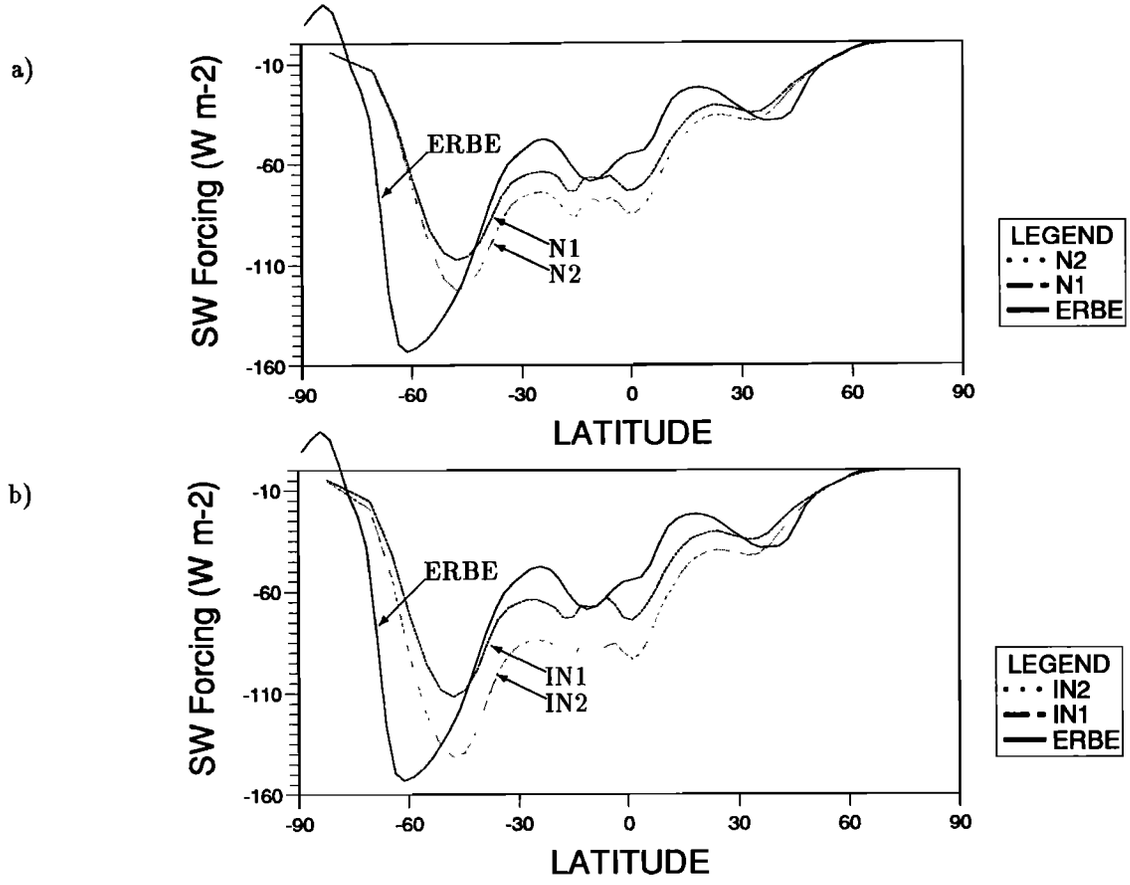

Figure 19. Zonal mean curves for the SW component of the CRF (watts per square meter) (a) for experiments N1 and N2, and (b) for experiments IN1 and IN2. Also shown is the ERBE data for a month of January.

seen that a fourfold increase in N leads to a significant increase in the SW cloud radiative forcing through a complex set of interactions, which simultaneously modify the cloud cover, the cloud water content, and the cloud droplet effective radius. About half of the extra forcing is due to a change in cloud droplet radius, and the other half from the associated changes in cloud water content and cloudiness. At this stage, these sensitivity experiments are academic since we prescribe the cloud droplet concentration, but the same model is being used for more applied scenarios: as we know, the number of CCNs may have changed since the beginning of the industrial period, in particular because of the release of sulfate aerosols [*Charlson et al.*, 1990; *Langner et al.*, 1992]. However, the computation of the cloud droplet concentration is still a challenging problem [*Boucher and Rodhe*, 1994; *Boucher and Lohmann*, 1995].

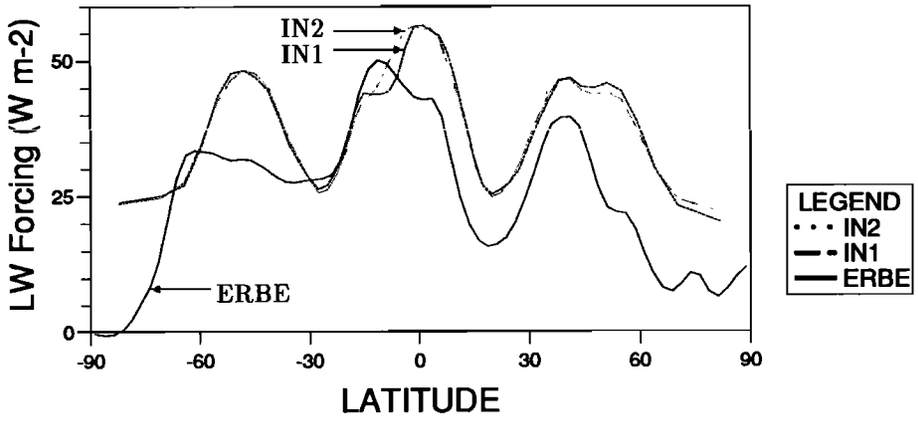

Figure 20. Zonal mean curves for the LW component of the CRF (watts per square meter): ERBE data and model.

As we have seen, it is difficult to reconcile clouds simulated by a large-scale model with what we know from observation and modeling of cloud microphysics. However our results are encouraging; improvements can be gained with a finer resolution (both horizontally and vertically) and/or subgrid scale distribution of cloud properties, such as the liquid water content [*Sommeria and Deardoff*, 1977; *Mellor*, 1977]. As stated in the model description, the parameterization of convection prevents from further developments of cloud microphysics. Also, the treatment of ice clouds is still very crude. This will be the subject of future work.

Notation List

c	multiplicative coefficient in the autoconversion rate.
E_r	rain evaporation rate, kg/kg s^{-1}.
$E(r, r')$	collection efficiency.
f	cloud fraction.
h	cloud thickness, m.
H	Heaviside step function.
l	in-cloud value of the cloud water mixing ratio, kg/kg.
$m(r)$	mass of a droplet with radius r, kg.
$M(R)$	mass of a raindrop with radius R, kg.
$n(r)$	cloud droplet radius distribution density, m^{-4}.
N	cloud droplet number concentration, m^{-3}.
$N(R)$	raindrop radius distribution density, m^{-4}.
$N(R) = N_0\, e^{-R/R_m}$.	
P	total precipitation rate, kg m^{-2} s^{-1}.
P_i	solid precipitation rate, kg m^{-2} s^{-1}.
P_l	liquid precipitation rate, kg m^{-2} s^{-1}.
q	grid box value of the water vapor mixing ratio, kg/kg.
q_{clear}	clear sky value of the water vapor mixing ratio, kg/kg.
q_l	grid box value of the cloud water mixing ratio, kg/kg.
q_r	grid box value of the rainwater mixing ratio, kg/kg.
q_{sat}	saturation over liquid water mixing ratio, kg/kg.
q_t	grid box value of the total water mixing ratio, kg/kg.
r	cloud droplet radius, m.
r_0	threshold cloud droplet radius, m.
r_c	effective cloud droplet radius for cold clouds, m.
r_e	effective cloud droplet radius, m.
r_w	effective cloud droplet radius for warm clouds, m.
$r_w = r_3{}^3/r_2{}^2$.	
r_n	equivalent radius for the n^{th} moment of the droplet radius distribution, m.
$r_n \equiv (\int r^n n(r)dr / \int n(r)dr)^{1/n}$.	
R	raindrop radius, m.
R_i	rate of release of ice crystals, kg/kg s^{-1}.
R_m	characteristic radius for the raindrop distribution, m.
R_{ll}	autoconversion rate, kg/kg s^{-1}.
R_{lr}	collection rate, kg/kg s^{-1}.
T	temperature, K.
$\boldsymbol{u}$	three-dimensional wind, m s^{-1}.
$V(r)$	terminal velocity of a cloud droplet with radius r, m s^{-1}.
$V(R)$	terminal velocity of a raindrop with radius R, m s^{-1}.
V_i	terminal velocity for solid hydrometeors, m s^{-1}.
V_r	mass-weighted average terminal velocity of the raindrop distribution, m s^{-1}.
W	liquid water path, kg m^{-2}.
x	proportion of liquid clouds as a function of temperature.
ϵ	cloud emissivity.
Γ	Gamma function.
ρ_0	air density in usual temperature and pressure conditions, kg m^{-3}.
ρ_{air}	air density, kg m^{-3}.
ρ_{water}	water density, kg m^{-3}.
τ	cloud optical depth.

Acknowledgments. We would like to thank Jan Polcher for his contribution to the development of this version of the model and Laurent Li for helpful discussion. J. Jensen and A. Blyth provided useful droplet spectral data from several cloud types. Computer time for numerical experiments was provided by the IDRIS (Institut du Développement et des Ressources en Informatique Scientifique). Olivier Boucher was partly supported by a grant from the Swedish Institute during the time of this study. M. Baker wishes to thank LMD for their hospitality and support and also to acknowledge partial support from NSF grant ATM-8907929. Support from the Environment project of the Commission of the European Communities is also acknowledged.

References

Albrecht, B. A., Aerosols, cloud microphysics, and fractional cloudiness, *Science*, *245*, 1227–1230, 1989.

Arking, A., The radiative effects of clouds and their impact on climate, *Bull. Am. Meteorol. Soc*, *71*, 795–813, 1991.

Baker, M. B., Variability in concentrations of CCN in the marine cloud-topped boundary layer, *Tellus*, *45B*, 458–472, 1993.

Beard, K. V., and H. T. Ochs III, Warm-rain initiation: An overview of microphysical mechanisms, *J. Appl. Meteorol.*, *32*, 608–625, 1993.

Bohren, C. F., Comment on "Cloud optical thickness feedbacks in the CO_2 climate problem" by Richard Sommerville and L. A. Remer, *J. Geophys. Res.*, *90*, 5867, 1985.

Boucher, O., and U. Lohmann, The sulfate-CCN-cloud albedo effect: A sensitivity study using two general circulation models, *Tellus*, *47B*, in press, 1995.

Boucher, O., and H. Rodhe, The sulfate-CCN-cloud albedo effect: A sensitivity study, *Rep. CM-83, Dep. of Meteorol., Stockholm University*, 20 pp., Jan. 1994.

Bower, K. N., T. W. Choularton, J. Latham, J. Nelson, M. Baker, J. Jensen, and A. Blyth, Microphysical properties of warm clouds, in *Proc. of the 11th Int. Conf. on Clouds and Precip.*, Vol. 1, 133–134, 1992.

Bower, K. N., T. W. Choularton, J. Latham, M. B. Baker, J. Jensen, and J. Nelson, A parameterisation of warm clouds for use in atmospheric general circulation models, *J. Atmos. Sci.*, *51*, 2722–2732, 1994.

Cess, R. D., and G. L. Potter, Exploratory studies of cloud radiative forcing with a general circulation model, *Tellus*, *39A*, 460–473, 1987.

Cess, R. D., et al., Intercomparison and interpretation of climate feedback processes in nineteen atmospheric general circulation models, *J. Geophys. Res.*, *95*, 16,601–16,615, 1990.

Charlock, T. P., and V. Ramanathan, The albedo field and cloud radiative forcing produced by a general circulation model with internally generated cloud optics, *J. Atmos. Sci.*, *42*, 1408–1429, 1985.

Charlson, R. J., J. E. Lovelock, M. O. Andreae, and S. G. Warren, Oceanic phytoplankton, atmospheric sulphur, cloud albedo and climate, *Nature*, *326*, 655–661, 1987.

Charlson, R. J., J. Langner, and H. Rodhe, Sulphate aerosol and climate, *Nature*, *348*, 22, 1990.

Charlson, R. J., S. E. Schwartz, J. M. Hales, R. D. Cess, J. A. Coakley, J. E. Hansen, and D. J. Hofmann, Climate forcing by anthropogenic aerosols, *Science*, *255*, 423–430, 1992.

Chen, C., and W. R. Cotton, The physics of the marine stratocumulus-capped mixed layer, *J. Atmos. Sci.*, *44*, 2951–2977, 1987.

Ducoudré, N. I., K. Laval, and A. Perrier, SECHIBA, a new set of parameterizations of the hydrologic exchanges at the land-atmosphere interface within the LMD atmospheric general circulation model, *J. of Clim.*, *6*, 248–273, 1993.

Fouquart, Y., and B. Bonnel, Computations of solar heating of the Earth's atmosphere: A new parameterization, *Beitr. Phys. Atmos.*, *53*, 35–62, 1980.

Fowler, L. D., D. A. Randall, and S. A. Rutledge, Liquid and ice cloud microphysics in the CSU general circulation model, I, Model description and simulated microphysical processes, *J. of Clim.*, in press, 1995.

Ghan, S. J., and R. C. Easter, Computationally efficient approximations to stratiform cloud microphysics parameterizations, *Mon. Weather Rev.*, *120*, 1572–1582, 1992.

Ghan, S. J., K. E. Taylor, J. E. Penner, and D. J. Erickson III, Model test of CCN-cloud albedo climate forcing, *Geophys. Res. Lett.*, *17*, 607–610, 1990.

Heymsfield, A. J., and L. J. Donner, A scheme for parameterizing ice-cloud water content in general circulation models, *J. Atmos. Sci.*, *47*, 1865–1877, 1990.

Hunt, B. G., An investigation with a general circulation model of the climatic effects of cloud albedo changes caused by atmospheric pollution, *J. Appl. Meteorol.*, *21*, 1071–1079, 1982.

International Panel on Climate Control (IPCC), *Climate Change: The IPCC Scientific Assessment*, edited by J. T. Houghton, G. J. Jenkins, and J. J. Ephraums, pp. 109, Cambridge University Press, New York, 1990.

Jaeger, L., Monatskarten des Niederschlags für die ganze Erde, *Bericht Deutscher Wetterdienst*, *18*, Nr. 139, 38 pp., 1976.

Kessler, E., *On the Distribution and Continuity of Water Substance in Atmospheric Circulation*, in *Meteorol. Monogr.*, vol. 10, 84 pp., Am. Meteorol. Soc., Mass., Boston, 1969.

Kiehl, J. T., Sensitivity of a GCM climate simulation to differences in continental versus maritime cloud drop size, *J. Geophys. Res.*, *99*, 23,107–23,115, 1994.

King, M. D., L. F. Radke, and P. V. Hobbs, Optical properties of marine stratocumulus clouds modified by ships, *J. Geophys. Res.*, *98*, 2729–2739, 1993.

Langner, J., H. Rodhe, P. J. Crutzen, and P. Zimmermann, Anthropogenic influence of the distribution of tropospheric sulphate aerosol, *Nature*, *359*, 712–716, 1992.

Legates, D. R., and C. J. Willmott, Mean seasonal and spatial variability in gauge-corrected, global precipitation, *Int. J. Climatol.*, *10*, 111–127, 1990.

Le Treut, H., and L. Illari, The inclusion of a cloud water continuity equation in a general circulation model: Sensitivity to the representation of the subgrid scale processes, in *Proc. of the International Radiation Symp. (IRS '92)*, edited by S. Keevallik and O. Kärner, 7–10, A. Deepak, Hampton, Va., 1993.

Le Treut, H., and Z. X. Li, Sensitivity of an atmospheric general circulation model to prescribed SST changes: Feedback effects associated with the simulation of cloud optical properties, *Clim. Dyn.*, *5*, 175–187, 1991.

Li, Z. X., and H. Le Treut, Sensitivity analysis with a 1-D climate model, (in English) *Chin. J. Atmos. Sci.*, *14*, 87–99, 1990.

Liou, K. N., and S. C. Ou, The role of cloud microphysical processes in climate: An assessment from a one-dimensional perspective, *J. Geophys. Res.*, *94*, 8599–8607, 1989.

Liu, J. Y., and H. D. Orville, Numerical modeling of precipitation and cloud shadow effects on mountain-induced cumuli, *J. Atmos. Sci.*, *26*, 1283–1298, 1969.

Marshall, J. S., and W. M. Palmer, The distribution of raindrops with size, *J. Meteorology*, *5*, 165–166, 1948.

Martin, G. M., D. W. Johnson, and A. Spice, The measurement and parameterization of effective radius droplets in warm stratocumulus clouds, *J. Atmos. Sci.*, *51*, 1823–1842, 1994.

Mellor, G. L., The gaussian cloud model relations, *J. Atmos. Sci.*, *34*, 356–358, 1977.

Morcrette, J. J., Radiation and cloud radiative properties in the European Centre for Medium Range Weather Forecasts forecasting system, *J. Geophys. Res.*, *96*, 9121–9132, 1991.

Ose, T., An examination of the effects of explicit cloud water in the UCLA GCM, *J. Meteorol. Soc. Jpn.*, *71*, 93–109, 1993.

Pruppacher, H. R., and J. D. Klett, *Microphysics of Clouds and Precipitation*, 714 pp., D. Reidel, Norwell, Mass., 1978.

Ramanathan, V., R. D. Cess, E. F. Harrison, P. Minnis, B. R. Barkstrom, E. Ahmad, and D. Hartmann, Cloud-radiative forcing and climate: Results from the Earth Radiation Budget Experiment, *Science*, *243*, 57–62, 1989.

Rogers, R. R., and M. K. Yau, *A Short Course in Cloud Physics*, 3rd ed., 293 pp., Pergamon, Tarry town, N. Y., 1989.

Sadourny, R., and K. Laval, January and July performance of the LMD general circulation model, in *New Perspectives in Climate Modelling*, pp. 173–198, edited by A. Berger and C. Nicolis, Elsevier, New York, 1984.

Schlesinger, M. E., J.-H. Oh, and D. Rosenfeld, A parameterization of the evaporation of rainfall, *Mon. Weather Rev.*, *116*, 1887–1895, 1988.

Slingo, A., Sensitivity of the Earth's radiation budget to changes in low clouds, *Nature*, *343*, 49–51, 1990.

Sommeria, G., and J. W. Deardoff, Subgrid-scale condensation in models of nonprecipitating clouds, *J. Atmos. Sci.*, *34*, 344–355, 1977.

Stephens, G. L., Radiation profiles in extended water clouds, I, Theory, *J. Atmos. Sci.*, *35*, 2111–2122, 1978.

Stephens, G. L., The parameterization of radiation for numerical weather prediction and climate models, *Mon. Weather Rev.*, *112*, 826–867, 1984.

Sun, Z., and K. P. Shine, Studies of the radiative properties of ice and mixed-phase clouds, *Q. J. R. Meteorol. Soc.*, *120*, 111–137, 1994.

Sundqvist, H., Parameterization of condensation and associated clouds in models for weather prediction and general circulation simulation, in *Physically-Based Modelling and Simulation of Climate and Climatic Change*, Part 1, 433–461, edited by M. E. Schlesinger, Kluwer Academic, Norwell, Mass., 1988.

Sundqvist, H., E. Berge, and J. E. Kristjánsson, Condensation and cloud parameterization studies with a mesoscale numerical weather prediction model, *Mon. Weather Rev.*, *117*, 1641–1657, 1989.

Tripoli, G. J., and W. R. Cotton, A numerical investigation of several factors contributing to the observed variable intensity of deep convection over South-Florida, *J. Appl. Meteorol.*, *19*, 1037–1063, 1980.

Twomey, S., Pollution and the planetary albedo, *Atmos. Environ.*, *8*, 1251–1256, 1974.

Twomey, S., The influence of pollution on the shortwave albedo of clouds, *J. Atmos. Sci.*, *34*, 1149–1152, 1977.

Twomey, S. A., M. Piepgrass, and T. Wolfe, An assessment of the impact of pollution on global cloud albedo, *Tellus*, *36B*, 356–366, 1984.

M. B. Baker, Geophysics Program, AK-50, University of Washington, Seattle, WA 98195
(e-mail: marcia@geophys.washington.edu).

O. Boucher and H. Le Treut, Laboratoire de Météorologie Dynamique du CNRS, Ecole Normale Supérieure, 24 rue Lhomond, 75231 Paris Cedex 05, France
(e-mail: boucher@lmd.ens.fr, letreut@lmd.ens.fr).

(Received November 23, 1993; revised January 31, 1995; accepted April 13, 1995.)